Method for obtaining polaron mobility using real and imaginary time path-integral quantum Monte Carlo

Suzana Miladić and Nenad Vukmirović*
Institute of Physics Belgrade, University of Belgrade, Pregrevica 118, 11080 Belgrade, Serbia

(Received 10 February 2023; revised 28 April 2023; accepted 23 May 2023; published 31 May 2023)

We developed a path-integral quantum Monte Carlo-based methodology for calculation of polaron mobility in systems with electron-phonon interaction. Within the method, the current-current correlation function in both the imaginary and real time is calculated in a numerically exact way. The choice of basis for representation of the path integral enabled us to reduce the sign problem and perform real-time calculations for longer times. The DC polaron mobility was extracted by performing analytic continuation that makes use of both the real and imaginary-time data. The method was applied to the Holstein polaron model in one dimension. We obtained reliable results for the temperature dependence of the Holstein polaron mobility for interactions ranging from weak to strong and temperatures that are not too low.

DOI: 10.1103/PhysRevB.107.184315

I. INTRODUCTION

The electron-phonon interaction is the dominant mechanism that determines the mobility of electrons or holes in semiconducting materials at room temperature [1,2]. There is a significant group of materials where it is sufficiently strong so that its perturbative treatment is not appropriate [3–5]. For such materials, one cannot apply the standard Bloch-Boltzmann theory [6] of electronic transport, nor the methods for mobility calculation based upon this theory that were developed in the last decade [6–12]. It is therefore of great interest to develop methods for the calculation of mobility of an electron interacting with phonons which would be applicable regardless of the strength of interaction.

The simplest model describing an electron interacting with phonons is the Holstein polaron model [13] where each lattice site accommodates one phonon and the electron interacts only locally with the phonon from the same site. This model served in the last several decades as a playground where the methods aiming at describing the systems with electron-phonon interaction were tested. Ground-state and equilibrium finite-temperature properties of the Holstein model are now well understood [14–25] and significant progress was recently made in evaluation of the electronic spectral function [26–30].

Nevertheless, it remains rather challenging to calculate the dynamical response of the system, which is encoded in real-time correlation functions in a numerically exact way; that is, without resorting to additional approximations in addition to those contained in the Hamiltonian. To calculate the DC polaron mobility one needs to calculate the current-current correlation function up to very long times. One of the methods to achieve this is to represent the current-current correlation function using Feynman's path integral formalism [31,32] and perform the calculation of the integral using a Monte Carlo method [24,33]. The main challenge comes from the fact that the sum obtained this way contains terms of varying phases. The Monte Carlo procedure for calculation of such a sum is then not guaranteed to converge. This issue constitutes the so-called dynamical sign problem [34–39]. The dynamical sign problem is not pronounced at small real times but it becomes severe at long times, making the calculations impossible. Other numerically exact methods that can in principle be used to evaluate real-time correlation functions include the finite-temperature Lanczos method [26], the time-dependent density-matrix renormalization-group method [28,40], and the hierarchical equations of motion method [29,41], whereas each of these exhibits its own challenges. There is also a significant number of approaches where the polaron transport in the Holstein and related models is evaluated by resorting to different types of approximations [42–57].

An approach that is often used to avoid the dynamical sign problem is to calculate the correlation functions in imaginary time or frequency and then perform the analytic continuation to real time or frequency [38,58–68]. However, such analytic continuation is an ill-posed problem and it gives reliable results in some cases only.

In this work, we perform path-integral quantum Monte Carlo calculations of the current-current correlation function in real and imaginary times for the Holstein model and we extract the DC mobility from these calculations. There are two main advances that we introduce in this work. First, we make use of the fact that the dynamical sign problem is basis-dependent [69]. By choosing the appropriate basis for the formulation of the path-integral quantum Monte Carlo method, we reduce the dynamical sign problem and enable the calculation of the current-current correlation function for longer times. Second, we perform the calculation of the current-current correlation function for both imaginary and (short) real times. To obtain the DC mobility, we then perform the analytic continuation, starting from both real and imaginary-time data. It is somewhat surprising that this simple

*nenad.vukmirovic@ipb.ac.rs

idea has rarely been exploited in the literature—we are in fact aware of only one work that exploited this idea [38]. The implementation of these ideas enabled us to obtain the mobility of the Holstein polaron for a broad range of parameters ranging from weak to strong interactions at temperatures that are not too low.

The paper is organized as follows: We briefly introduce the model Hamiltonian in Sec. II A. In Sec. II B we derive the path-integral representation of the current-current correlation function in two different bases and describe the numerical Monte Carlo algorithms for its calculation. In Sec. II C we present the procedure for analytic continuation that makes use of both real and imaginary-time data to obtain the DC mobility. An example of the application of the analytic continuation procedure is presented in Sec. III A. Convergence tests of our numerical calculations are presented in Sec. III B. The final results for the temperature dependence of the Holstein polaron mobility are presented in Sec. III C, while concluding remarks are given in Sec. IV.

II. MODEL AND METHODS

A. Model Hamiltonian

We consider the system described by the Holstein model on an one-dimensional lattice. Each lattice site accommodates one phonon mode. An electron interacts locally with the phonon. The system is described by the Hamiltonian

$$H = \sum_n \Big[-J\left(c_n^\dagger c_{n+1} + c_{n+1}^\dagger c_n\right) + \left(\frac{P_n^2}{2M} + \frac{1}{2}M\omega_n^2 X_n^2\right) + \sqrt{2M\omega_n}\, G c_n^\dagger c_n X_n \Big]. \tag{1}$$

The first term describes electron hopping on the lattice, where J is the electronic transfer integral between neighboring sites. The operators $c_n^\dagger$ (c_n) stand for electron creation (annihilation) operators at the nth site. The second term describes the phonon of angular frequency ω_n, while X_n (P_n) are phonon position (momentum) operators at site n. Dispersionless phonons with $\omega_n = \omega_0$ are assumed. The mass M of the oscillator can be set to $M = 1$ without loss of generality. The last term describes the electron-phonon interactions of strength G. We assume periodic boundary conditions. In the derivations throughout the paper we use the system of units where the lattice constant a and the universal physical constants $\hbar$, e_0, and k_B are equal to 1. We denote the inverse temperature as $\beta = 1/T$.

The Hamiltonian given in Eq. (1) can be written in the following equivalent form, which is more suitable for the derivation of the path integral representation:

$$H = H_0 + H_1 + H_2, \tag{2a}$$

$$H_0 = \sum_n \frac{P_n^2}{2M}, \tag{2b}$$

$$H_1 = \sum_n \left(\sqrt{2M\omega_n}\, G c_n^\dagger c_n X_n + \frac{1}{2}M\omega_n^2 X_n^2\right), \tag{2c}$$

$$H_2 = -J\sum_n (c_n^\dagger c_{n+1} + c_{n+1}^\dagger c_n). \tag{2d}$$

The Hamiltonian H_2 is diagonal in electron momentum representation $H_2 = \sum_k \varepsilon(k) c_k^\dagger c_k$, where the bare electronic dispersion is given as $\varepsilon(k) = -2J\cos(k)$ and $c_k^\dagger$ (c_k) are the electron creation (annihilation) operators in the momentum representation.

B. Path-integral representation of time-correlation functions

The central quantity that we consider in this work is the DC mobility which is given by the Kubo formula [42,70]

$$\mu = \frac{\beta}{2}\int_{-\infty}^{\infty} dt\, \langle j(t) j(0)\rangle, \tag{3}$$

where the current-density operator j for the Holstein model reads

$$j = iJ\sum_n (c_n^\dagger c_{n+1} - c_{n+1}^\dagger c_n). \tag{4}$$

To evaluate the mobility, one needs to calculate the time-correlation function (TCF) $\langle j(t) j(0)\rangle$, where the brackets denote the average in the canonical ensemble.

The TCF that corresponds to arbitrary operators A and B is by definition

$$\langle A(t) B\rangle = Z^{-1}\mathrm{Tr}[e^{-\beta H} e^{itH} A e^{-itH} B], \tag{5}$$

where $Z = \mathrm{Tr}(e^{-\beta H})$ is the partition function and the time dependence of the operators is given as $A(t) = e^{itH} A e^{-itH}$ with $A(0) \equiv A$. To derive a discretized path-integral representation of the TCF given in Eq. (5), we make use of the Trotter-Suzuki expansion in accordance with the ideas from Refs. [24,33]:

$$\langle A(t) B\rangle = \lim_{m,Q\to\infty} Z_m^{-1}\mathrm{Tr}[(e^{-\tau H_0} e^{-\tau H_1} e^{-\tau H_2})^m (e^{i\Delta t H_0} \times e^{i\Delta t H_1} e^{i\Delta t H_2})^Q A (e^{-i\Delta t H_0} e^{-i\Delta t H_1} e^{-i\Delta t H_2})^Q B], \tag{6}$$

The imaginary-time interval of length β was divided into m subintervals of length $\tau = \beta/m$, while the real-time interval of length t was divided into Q subintervals of length $\Delta t = t/Q$. The term Z_m is the partition function that is obtained when the imaginary-time interval is divided into m subintervals.

The trace in Eq. (6) can be evaluated by representing it in any complete basis that spans the Hilbert space of the system. The result of the full summation does not depend on the choice of basis. However, the result and the statistical error of Monte Carlo summation, which includes only a sample of the terms in the sum, depends on the choice of basis. This fact can be exploited to choose a basis where the statistical error of Monte Carlo summation is smaller. In practice, this enables us to perform calculations for longer real times than if only one choice of basis were used. We made use of two possibilities for the choice of basis: (i) the basis obtained as a direct product of electronic momentum states and phonon coordinate eigenstates; (ii) the basis obtained as a direct product of the electronic states with an electron localized at a certain site and phonon coordinate eigenstates. The choice (i) is more natural for weak electron-phonon interaction, while we make use of (ii) for stronger electron-phonon interaction and for

imaginary-time calculations. It should be noted that the choice (ii) allows us to analytically integrate out phononic degrees of freedom.

We consider both the real time correlation function as defined in Eq. (5) and the imaginary time correlation function (obtained by the Wick rotation $t \to -it, t \in \mathbb{R}$) given by

$$\langle A(-it)B\rangle = Z^{-1}\mathrm{Tr}[e^{-\beta H}e^{tH}Ae^{-tH}B]. \tag{7}$$

We denote the trace appearing in Eq. (6) as $C^{m,Q}_{A,B}$ and in the next two sections we derive its path-integral representation in the two bases mentioned. In the derivation, we assume that the operators A and B depend on electronic degrees of freedom only, which is the case for the current-density operator for the Holstein model given in Eq. (4).

1. Path integral with momentum representation for electrons

We expand the trace from Eq. (6) in the basis containing the states that are a direct product of electron momentum states and phonon coordinate eigenstates:

$$|k;\{X\}\rangle = |k\rangle|X_0\rangle|X_1\rangle\cdots|X_{N-1}\rangle, \tag{8}$$

where N is the number of sites in the lattice. The electron momentum k takes one of N discrete values from the first Brillouin zone, while phonon coordinates are real numbers. To obtain a discretized representation of the path integral, we evaluate the trace $C^{m,Q}_{A,B}$ in the basis given in Eq. (8). The details of the derivation are given in Sec. I of the Supplemental Material [71]. We arrive at the expression:

$$\begin{aligned} C^{m,Q}_{A,B} = C_1' \int \prod_{j=0}^{m-1} \mathrm{D}X^j \prod_{p=m}^{m+Q} \mathrm{D}X^p \prod_{r=m+Q+1}^{m+2Q+1} \mathrm{D}X^r e^{-S_1[\tau;X^j]} e^{-S_2[-i\Delta t;X^p]} e^{-S_3[i\Delta t;X^r]} \\ \times \sum_{\{k\}} \prod_{j=0}^{m-1} f_{k_{j+1},k_j}(-\tau;X^{j+1}) \prod_{p=m}^{m+Q-1} f_{k_{p+1},k_p}(i\Delta t;X^{p+1}) \prod_{r=m+Q+1}^{m+2Q} f_{k_{r+1},k_r}(-i\Delta t;X^{r+1}) \\ \times \langle X^{m+Q};k_{m+Q}|A|k_{m+Q+1};X^{m+Q+1}\rangle\langle X^{m+2Q+1};k_{m+2Q+1}|B|k_0;X^0\rangle, \end{aligned} \tag{9}$$

where C_1' is an irrelevant constant and $\sum_{\{k\}}$ denotes the summation over all k variables. Phonon actions are given by the expressions

$$\begin{aligned} S_1[\tau;X^j] &= \tau \sum_{j=0}^{m-1} \sum_n \left[\frac{M}{2}\omega_n^2 \left(X_n^{j+1}\right)^2 + \frac{M}{2}\frac{\left(X_n^{j+1}-X_n^j\right)^2}{\tau^2} \right], \\ S_2[-i\Delta t;X^p] &= -i\Delta t \sum_{p=m}^{m+Q-1} \sum_n \left[\frac{M}{2}\omega_n^2 \left(X_n^{p+1}\right)^2 + \frac{M}{2}\frac{\left(X_n^{p+1}-X_n^p\right)^2}{(i\Delta t)^2} \right], \\ S_3[i\Delta t;X^r] &= i\Delta t \sum_{r=m+Q+1}^{m+2Q} \sum_n \left[\frac{M}{2}\omega_n^2 \left(X_n^{r+1}\right)^2 + \frac{M}{2}\frac{\left(X_n^{r+1}-X_n^r\right)^2}{(i\Delta t)^2} \right]. \end{aligned} \tag{10}$$

The functions $f_{k_i,k_j}(z;x^i)$ are fermion propagators between states k_i and k_j in complex time z and are defined as

$$f_{k_i,k_j}(z;X^i) = e^{z\varepsilon(k_i)}\frac{1}{N}\sum_n e^{in\cdot(k_i-k_j)+zG\sqrt{2M\omega_n}X_n^i}. \tag{11}$$

The estimator for the TCF is given by the expression

$$\langle A(t)B\rangle^{m,Q} = \frac{C^{m,Q}_{A,B}}{C^{m,Q}_{1,1}}, \tag{12}$$

where the term $C^{m,Q}_{1,1}$ denotes $C^{m,Q}_{A,B}$ for $A = B = 1$. The estimator from Eq. (12) closely represents the true correlation function $\langle A(t)B\rangle$ when m and Q are large enough.

We rewrite the trace $C^{m,Q}_{A,B}$ in matrix notation by introducing the vector variable for phonon coordinates:

$$\begin{aligned} \mathbf{Y} = (Y^0, Y^1, \ldots, Y^{m+2Q-1})^T = (X^1, X^2, \ldots, X^{m+Q-1}, \\ X^{m+Q+1}, \ldots, X^{m+2Q-1}, X^{m+2Q}, X^0)^T, \end{aligned} \tag{13}$$

so the trace takes form

$$C^{m,Q}_{A,B} = C_1' \int \mathrm{D}\mathbf{Y} e^{-\frac{1}{2}\mathbf{Y}^T\mathcal{D}\mathbf{Y}} F(\mathbf{Y}). \tag{14}$$

The matrix $\mathcal{D}$ is a symmetric matrix that represents the quadratic form in the phonon actions. The function $F(\mathbf{Y})$ is a trace of the product of matrices

$$\begin{aligned} F(\mathbf{Y}) = \mathrm{Tr}[&\mathcal{F}(-\tau;Y^0)\mathcal{F}(-\tau;Y^1)\ldots\mathcal{F}(-\tau;Y^{m-1}) \\ &\times \mathcal{F}(i\Delta t;Y^m)\cdots\mathcal{F}(i\Delta t;Y^{m+Q-2}) \\ &\times \mathcal{G}(i\Delta t;Y^{m+Q-1})\mathcal{F}(-i\Delta t;Y^{m+Q})\cdots \\ &\times \mathcal{F}(-i\Delta t;Y^{m+2Q-2})\mathcal{G}(-i\Delta t;Y^{m+2Q-1})] \end{aligned} \tag{15}$$

When $A = B = j$ the elements of the matrices are given as

$$[\mathcal{F}(z;Y^k)]_{l,j} = e^{z\varepsilon(2\pi j/N)}\frac{1}{N}\sum_{n=0}^{N-1} e^{-in\cdot(j-l)\frac{2\pi}{N}+zG\sqrt{2\omega_0}Y_n^k},$$

$$[\mathcal{G}(i\Delta t;Y^{m+Q-1})]_{l,j} = -2J\sin(2\pi j/N)e^{i\Delta t\varepsilon(2\pi j/N)}\frac{1}{N}\sum_{n=0}^{N-1} e^{-in\cdot(j-l)\frac{2\pi}{N}+i\Delta tG\sqrt{2\omega_0}Y_n^{m+Q-1}},$$

$$[\mathcal{G}(-i\Delta t;Y^{m+2Q-1})]_{l,j} = -2J\sin(2\pi j/N)e^{-i\Delta t\varepsilon(2\pi j/N)}\frac{1}{N}\sum_{n=0}^{N-1} e^{-in\cdot(j-l)\frac{2\pi}{N}-i\Delta tG\sqrt{2\omega_0}Y_n^{m+2Q-1}}, \tag{16}$$

where z is complex time. When $A = B = 1$, the matrices $\mathcal{G}$ should be simply replaced by matrices $\mathcal{F}$.

We calculate the integrals that appear in $C_{A,B}^{m,Q}$ using a Monte Carlo technique by directly sampling from phonon action

$$S[\mathbf{Y}] = \tfrac{1}{2}\mathbf{Y}^T\mathcal{D}\mathbf{Y}. \tag{17}$$

Since $\mathcal{D}$ is a complex symmetric matrix, we can diagonalize the quadratic form $\mathbf{Y}^T\mathcal{D}\mathbf{Y}$ by eigen decomposition $\mathcal{D} = Q\Lambda Q^{-1}$, where Λ is a diagonal matrix and Q is an orthogonal matrix $Q^T = Q^{-1}$. The quadratic form then takes the form $\mathbf{Y}^T\mathcal{D}\mathbf{Y} = \mathbf{Z}^T\mathbf{Z}$. We can therefore directly sample the components Z_k from a Gaussian distribution and find the vectors $\mathbf{Y}$ by applying an inverse transformation $\mathbf{Y} = Q^T\Lambda^{-1/2}\mathbf{Z}$.

2. *Path integral with position representation for electrons*

In this case we make use of the basis consisting of states that are a direct product of electron position states and phonon coordinate eigenstates,

$$|r;\{X\}\rangle = |r\rangle|X_0\rangle|X_1\rangle\cdots|X_{N-1}\rangle, \tag{18}$$

The electron position takes the values $r = 0,\ldots,N-1$. Following the same procedure as in Sec. II B 1, we arrive at a similar expression for the trace $C_{A,B}^{m,Q}$ in this basis, where the details of the derivation are given in Sec. II of the Supplemental Material [71]:

$$\begin{aligned} C_{A,B}^{m,Q} = {} & C_2'\sum_{\{r\}}\langle r_{m+Q}|A|r_{m+Q+1}\rangle\langle r_{m+2Q+1}|B|r_0\rangle \\ & \times\prod_{j=0}^{m-1} I(\tau;r_{j+1}-r_j)\prod_{p=m}^{m+Q-1} I(-i\Delta t;r_{p+1}-r_p) \\ & \times\prod_{q=m+Q+1}^{m+2Q} I\big(i\Delta t;r_{q+1}-r_q\big) \\ & \times\int\prod_{j=0}^{m-1}\mathrm{D}X^j\prod_{p=m}^{m+Q-1}\mathrm{D}X^p\prod_{q=m+Q+1}^{m+2Q}\mathrm{D}X^q \\ & \times e^{-S_1[\tau;X^j]}e^{-S_2[-i\Delta t;X^p]}e^{-S_3[i\Delta t;X^q]}, \end{aligned} \tag{19}$$

where C_2' is an irrelevant constant, the symbol $\sum_{\{r\}}$ denotes the summation over all r variables and phonon actions are given by the expressions

$$\begin{aligned} S_1[\tau;X^j] = {} & \tau\sum_{j=0}^{m-1}\sum_n\left[\frac{M}{2}\omega_n^2\big(X_n^{j+1}\big)^2\right. \\ & \left.+\frac{M}{2}\frac{\big(X_n^{j+1}-X_n^j\big)^2}{\tau^2}+G\sqrt{2M\omega_n}\delta_{n,r_j}X_n^{j+1}\right], \\ S_2[-i\Delta t;X^p] = {} & -i\Delta t\sum_{p=m}^{m+Q-1}\sum_n\left[\frac{M}{2}\omega_n^2\big(X_n^{p+1}\big)^2\right. \\ & \left.+\frac{M}{2}\frac{\big(X_n^{p+1}-X_n^p\big)^2}{(i\Delta t)^2}+G\sqrt{2M\omega_n}\delta_{n,r_p}X_n^{p+1}\right], \\ S_3[i\Delta t;X^q] = {} & i\Delta t\sum_{q=m+Q+1}^{m+2Q}\sum_n\left[\frac{M}{2}\omega_n^2\big(X_n^{q+1}\big)^2\right. \\ & \left.+\frac{M}{2}\frac{\big(X_n^{q+1}-X_n^q\big)^2}{(i\Delta t)^2}+G\sqrt{2M\omega_n}\delta_{n,r_q}X_n^{q+1}\right]. \end{aligned} \tag{20}$$

The functions $I(z;r_{j+1}-r_j)$ represent Fourier-transformed electron propagators to coordinate space and they are defined as [24]

$$\begin{aligned} I\big(z;r_{j+1}-r_j\big) = {} & \frac{1}{N}\sum_{n=0}^{N-1}\cos\left(\frac{2\pi}{N}n\big(r_{j+1}-r_j\big)\right) \\ & \times\exp\left[2zJ\cos(2\pi n/N)\right]. \end{aligned} \tag{21}$$

The integral over phonon coordinates in Eq. (19) can be solved analytically. As in the previous section, we introduce the vector variable for phonon coordinates which leads to

$$\begin{aligned} f(\{r\}) = {} & \int\prod_{j=0}^{m-1}\mathrm{D}X^j\prod_{p=m}^{m+Q-1}\mathrm{D}X^p\prod_{q=m+Q+1}^{m+2Q}\mathrm{D}X^q \\ & \times e^{-S_1[\tau;X^j]}e^{-S_2[-i\Delta t;X^p]}e^{-S_3[i\Delta t;X^q]} \\ = {} & \int\mathrm{D}\mathbf{Y}e^{-S[\mathbf{Y}]}, \end{aligned} \tag{22}$$

where $\mathbf{Y}$ is given in Eq. (13) and the action is a quadratic form with an additional linear term

$$S[\mathbf{Y}] = \tfrac{1}{2}\mathbf{Y}^T\mathcal{D}\mathbf{Y}+\mathbf{Y}^T\cdot\mathbf{d}(\{r\}). \tag{23}$$

The matrix $\mathcal{D}$ is the same as in Sec. II B 1, while the vector $\mathbf{d}(\{r\})$ depends on the configuration of electron position states. After calculating the multidimensional Gaussian integral over phonon states we obtain the function $f(\{r\})$ that depends on electron position states

$$f(\{r\}) = C_3' \exp\left(\tfrac{1}{2}\mathbf{d}(\{r\})^T \cdot \mathcal{D}^{-1} \cdot \mathbf{d}(\{r\})\right), \tag{24}$$

where C_3' is an irrelevant constant that remains after Gaussian integration.

The trace $C_{A,B}^{m,Q}$ is in this case given as

$$C_{A,B}^{m,Q} = C_2' C_3' \sum_{\{r\}} w(\{r\}) F(\{r\}), \tag{25}$$

where we introduced the weight function $w(\{r\})$ and the function $F(\{r\})$ given by the expressions

$$w(\{r\}) = \prod_{j=0}^{m-1} I\left(\tau; r_{j+1} - r_j\right) \prod_{p=m}^{m+Q-1} |I(-i\Delta t; r_{p+1} - r_p)| \times \prod_{q=m+Q+1}^{m+2Q} |I(i\Delta t; r_{q+1} - r_q)|, \tag{26}$$

$$F(\{r\}) = \langle r_{m+Q}|A|r_{m+Q+1}\rangle \langle r_{m+2Q+1}|B|r_0\rangle \times \exp\left(\frac{1}{2}\mathbf{d}(\{r\})^T \cdot \mathcal{D}^{-1} \cdot \mathbf{d}(\{r\})\right) \times \prod_{p=m}^{m+Q-1} e^{i\phi(-i\Delta t; r_{p+1} - r_p)} \prod_{q=m+Q+1}^{m+2Q} e^{i\phi(i\Delta t; r_{q+1} - r_q)}, \tag{27}$$

where $\phi(z; r_i - r_j) = \arg[I(z; r_i - r_j)]$.

To calculate the real-time correlation function we use the same estimator $\langle A(t)B\rangle^{m,Q}$ as in Eq. (12). The sum in Eq. (25) over electron position states will be calculated by using the Monte Carlo technique. After a simple change of variables r_j, the weight $w(\{r\})$ becomes a product of single-variable functions. These variables can then be sampled independently to obtain the configuration of electron positions $\{r\}$.

To obtain the path integral in imaginary time, we can simply make the substitution $t \to -it$ in expressions obtained in real time. The weight from Eq. (26) and the function from Eq. (27) are now completely real and are given by the expressions:

$$w(\{r\}) = \prod_{j=0}^{m-1} I\left(\tau; r_{j+1} - r_j\right) \prod_{p=m}^{m+Q-1} I(-\Delta t; r_{p+1} - r_p) \times \prod_{q=m+Q+1}^{m+2Q} I(\Delta t; r_{q+1} - r_q), \tag{28}$$

$$F(\{r\}) = \langle r_{m+Q}|A|r_{m+Q+1}\rangle \langle r_{m+2Q+1}|B|r_0\rangle \times \exp\left(\frac{1}{2}\mathbf{d}(\{r\})^T \cdot \mathcal{D}^{-1} \cdot \mathbf{d}(\{r\})\right). \tag{29}$$

C. Analytic continuation

The path-integral quantum Monte Carlo methodology described in Sec. II B gives us the current-current correlation function $\langle j(t_c)j(0)\rangle$ either at imaginary times ($t_c = -it$, $0 \leqslant t \leqslant \beta$) or at short real times ($t_c = t$). On the other hand, the central quantity that we are interested in is the DC mobility $\mu = \mu(\omega = 0)$. The relation between $\langle j(t_c)j(0)\rangle$ and $\mu(\omega)$ reads

$$\langle j(t_c)j(0)\rangle = \int_{-\infty}^{\infty} d\omega \frac{1}{\pi} \frac{\omega e^{-i\omega t_c}}{1 - e^{-\beta\omega}} \mathrm{Re}\mu(\omega). \tag{30}$$

This type of problem is in the quantum many body community typically addressed by calculating the correlation function [in our case $\langle j(t_c)j(0)\rangle$] at imaginary times where there is no sign problem and then performing analytic continuation to obtain $\mathrm{Re}\mu(\omega)$. The methods that are typically used to perform analytic continuation include the maximum entropy method [38,58,59,63,65–67], the Padé approximation method [59–61], the singular-value decomposition method [59,63,64], etc.

However, one can also make use of the calculations for those real times where the sign problem is not pronounced and accurate values of the current-current correlation function can be obtained. Therefore, we perform analytic continuation by making use of both imaginary-time and real-time data obtained by path-integral Monte Carlo calculations of the current-current correlation function.

We make use of the singular-value decomposition method to perform analytic continuation. The discretized version of Eq. (30) reads

$$\mathbf{j} = \mathbf{K} \cdot \mathbf{m}, \tag{31}$$

where $\mathbf{K}$ is a known linear operator obtained from discretization of Eq. (30). The vector $\mathbf{j}$ contains the current-current correlation function for all (real or imaginary) times at which calculations were performed. The vector $\mathbf{m}$ is unknown and it contains the discrete representation of $\mathrm{Re}\mu(\omega)$. All the elements of $\mathbf{j}$, $\mathbf{K}$, and $\mathbf{m}$ are real if we represent complex numbers as a column of two real numbers—their real and imaginary part. Any real matrix can be transformed to the form known as singular-value decomposition:

$$\mathbf{K} = \mathbf{U}\mathbf{S}\mathbf{V}^T, \tag{32}$$

where $\mathbf{U}$ and $\mathbf{V}$ are orthogonal matrices, while $\mathbf{S}$ is a diagonal matrix whose elements s_k are called the singular values. Within the singular-value decomposition method we find $\mathbf{m}$ as

$$\mathbf{m} = \sum_k \frac{\mathbf{U}_{.,k}^T \cdot \mathbf{j}}{s_k} \mathbf{V}_{.,k}, \tag{33}$$

where $\mathbf{U}_{.,k}^T$ ($\mathbf{V}_{.,k}$) is the kth column vector of matrix $\mathbf{U}^T$ ($\mathbf{V}$).

The challenge in obtaining $\mathbf{m}$ from Eq. (33) comes from the fact that there are many singular values that are close to zero. The presence of such values leads to large multiplication of any noise (stemming from Monte Carlo data or from finite numerical precision). Therefore, in practice one takes only a limited number of terms in Eq. (33) that correspond to largest values of s_k.

We note that analytic continuation that includes both real- and imaginary-time data is by no means limited to the singular-value decomposition method. It can be performed by appropriate modification of any other analytic continuation method. We nevertheless chose the singular-value decompo-

sition method because it most transparently demonstrates the challenges of analytic continuation procedure.

III. RESULTS

A. Examples of analytic continuation procedure

In this section, we present examples of the results obtained from our analytic continuation procedure. To assess the accuracy and limitations of the procedure, it is desirable to know the exact reference result for $\mu(\omega)$ that the procedure should ideally reconstruct. For this reason, here we do not apply the procedure to our Monte Carlo data. Instead, we make use of the frequency dependence of mobility obtained in Ref. [72] that we refer to as the reference dynamic mobility $\mu_{\text{ref}}(\omega)$. From the reference dynamic mobility, we construct the real- and imaginary-time current-current correlation functions using Eq. (30). Next, we add noise to these data whose strength is comparable to the noise present in our Monte Carlo data. Finally, we apply the analytic continuation procedure described in Sec. II C to such data and obtain $\text{Re}\mu_{\text{ac}}(\omega)$. By comparing $\text{Re}\mu_{\text{ac}}(\omega)$ and $\text{Re}\mu_{\text{ref}}(\omega)$ we can estimate the accuracy of the analytic continuation procedure. Since we are mostly interested in DC mobility we make the comparison in particular at $\omega = 0$. We use the relative error

$$\delta = \frac{\text{Re}\mu_{\text{ac}}(\omega = 0) - \text{Re}\mu_{\text{ref}}(\omega = 0)}{\text{Re}\mu_{\text{ref}}(\omega = 0)}$$

as an estimate of the error of analytic continuation procedure.

The results are presented for model parameters $\omega_0/J = 1$, $G/J = 1$ and $T/J = 1$ in Fig. 1(a). These results were obtained from imaginary-time data for times up to $0.6/J$ and real-time data for times up to $1/J$, while the results in Fig. 1(b) are obtained from same imaginary-time data with the addition of real-time data with ranges specified in the caption of the figure.

In Fig. 1(a) we demonstrate how the number of singular values (svs) taken in the sum given by Eq. (33) affects the outcome of analytic continuation. If we take too many svs terms (e.g., svs = 13), we include the term with rather small absolute value of s_k in Eq. (33). The noise in the data $\mathbf{j}$ in Eq. (33) is then strongly multiplied and we get too much noise in the $\text{Re}\mu_{\text{ac}}(\omega)$. On the other hand, if we take too few singular values (e.g., svs = 8, 9) we do not have enough information and $\text{Re}\mu_{\text{ac}}(\omega)$ does not resemble the reference $\text{Re}\mu_{\text{ref}}(\omega)$ at all. The best choice in practice is to take as many singular values as possible before $\text{Re}\mu_{\text{ac}}(\omega)$ becomes too noisy. For the specific case shown in Fig. 1(a) the best choice is the result obtained with 12 singular values. The number of singular values used in typical calculations in this work is reported in the table in Sec. III of the Supplemental Material [71].

In Fig. 1(b) we demonstrate the benefits of performing analytic continuation starting both from real- and imaginary-time data as opposed to using the imaginary-time data only. By adding more relevant data in real time, we get closer to the reference result in comparison with the case when we use imaginary-time data only. We can see that, by combining imaginary- and real-time data, we can get much closer to the reference value of mobility.

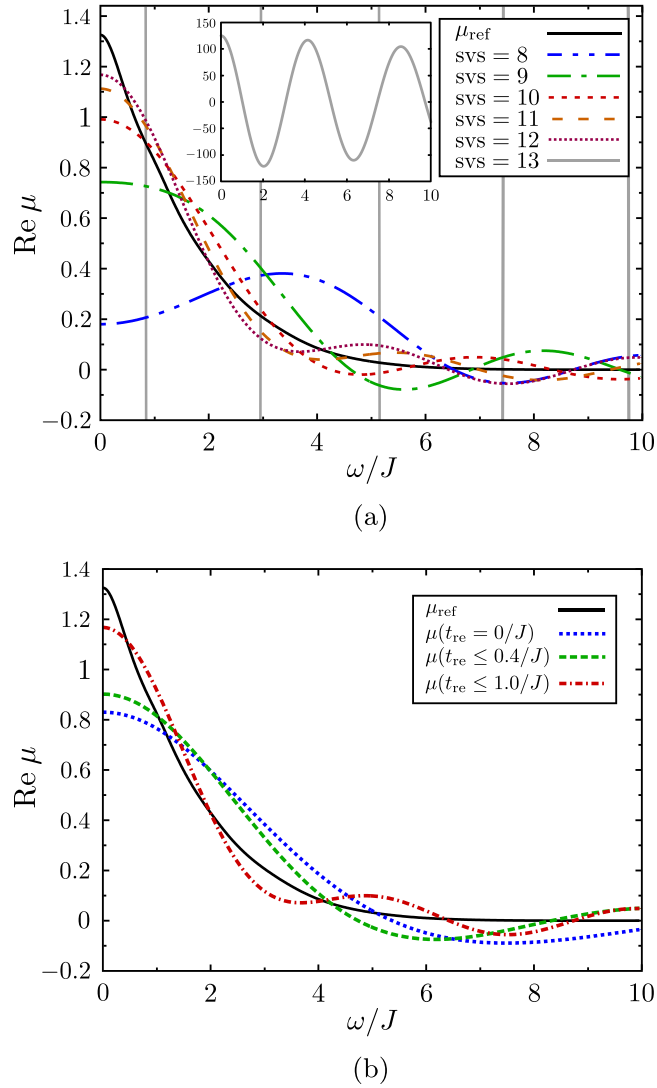

FIG. 1. Examples of the application of the analytic continuation procedure: (a) The reference result (labeled μ_{ref}) and the results obtained using different number of singular values (svs). The inset shows the result obtained using svs = 13 with a full range on the y axis; (b) The reference result (μ_{ref}) and the results obtained using imaginary-time data only [labeled $\mu(t_{\text{re}} = 0)$], using imaginary-time data and real-time data for real times up to $0.4/J$ [labeled $\mu(t_{\text{re}} \leqslant 0.4/J)$] and using imaginary-time data and real-time data for real times up to $1/J$ [labeled $\mu(t_{\text{re}} \leqslant 1.0/J)$]. The results are presented for model parameters $\omega_0/J = 1$, $G/J = 1$ and $T/J = 1$. The results are shown for $\omega \geqslant 0$ because the equality $\text{Re}\mu(\omega) = \text{Re}\mu(-\omega)$ holds.

B. Choice of simulation parameters

To make sure that the results of our quantum Monte Carlo calculations are reliable, we paid particular attention to set the appropriate values of all relevant simulation parameters. Relevant convergence tests were performed to choose these values. Since our goal is to get very precise data such that standard deviation is not greater than 1% of the result, we used 10^4–10^6 Monte Carlo samples in a single calculation and we repeat each calculation 100 times to achieve better statistics and to estimate the statistical error. The discretization time

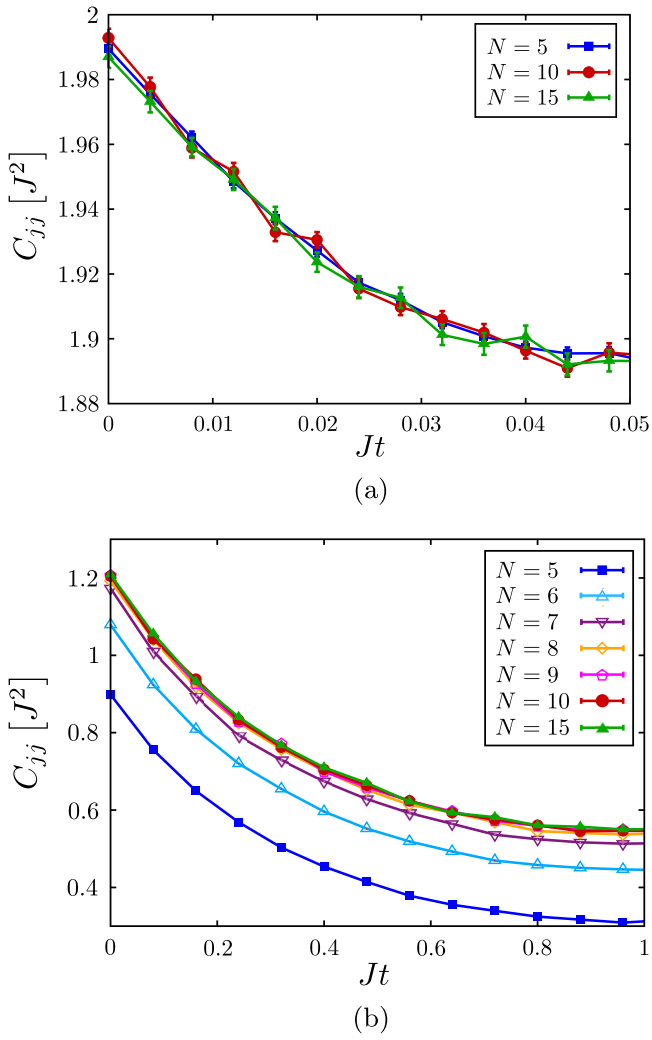

FIG. 2. The dependence of the imaginary-time current-current correlation function on the number of sites N for $\omega_0/J = 1$ and $G/J = 1$: (a) at a high temperature $T/J = 10$, (b) at a low temperature $T/J = 0.5$. The results are shown for imaginary times $0 \leqslant t \leqslant \beta/2$ only since the identity $C_{jj}(t) = C_{jj}(\beta - t)$ holds. The error bars in panel (a) of the figure denote the estimated standard deviation of the result, while the error is too small to be visible in panel (b) of the graph.

steps τ and Δt also have to be set to particular values. From appropriate convergence tests, we found that the values $\tau = \Delta t = \frac{0.1}{J}$ are small enough as taking smaller time steps does not make a significant change in the result. Time discretization steps and the number of Monte Carlo samples used in typical calculations in this work are given in the table in Sec. III of the Supplemental Material [71].

Another relevant parameter is the number N of sites that determines the system size. Our goal is to obtain the results representative of the thermodynamic limit $N \to \infty$. In practice, we thus choose N which is large enough so that further increase in the number of sites does not change the result. In Figs. 2(a) and 2(b) we present the imaginary-time current-current correlation function for $\omega_0/J = 1$ and $G/J = 1$ at a high temperature $T/J = 10$ and a low temperature $T/J = 0.5$ for a different number N of sites. We see that, for these

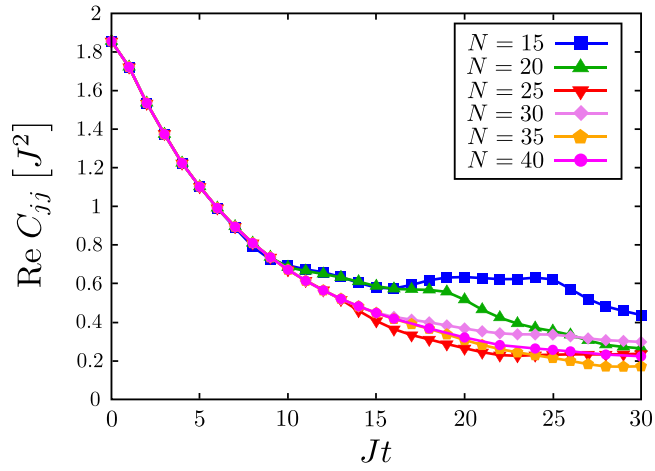

FIG. 3. Real part of real-time current-current correlation function for different number N of sites for $G/J = 0.141$, $\omega_0/J = 1$, and $T/J = 2.5$.

parameters, $N = 5$ sites are sufficient at a high temperature, while $N = 10$ sites are needed at a low temperature. Such behavior is expected since the increase in temperature reduces spatial correlations. For this reason, the system becomes more local at a higher temperature and a smaller number of sites is needed to reach the thermodynamic limit.

In Fig. 3 we present the time dependence of the real part of current-current correlation function in real time obtained through Monte Carlo calculations for various system sizes in the case of weak electron-phonon interaction $G/J = 0.141$, $\omega_0/J = 1$, and $T/J = 2.5$. We see from the figure that a system of $N = 30$ sites is needed for accurate calculation for times up to $Jt = 15$. Such a large N is needed in this case because the carrier mean-free path is large for weak electron-phonon interaction and the system size larger than the carrier mean-free path is needed to obtain the result representative of the thermodynamic limit. To reduce the computational effort we performed the calculation for smaller times with

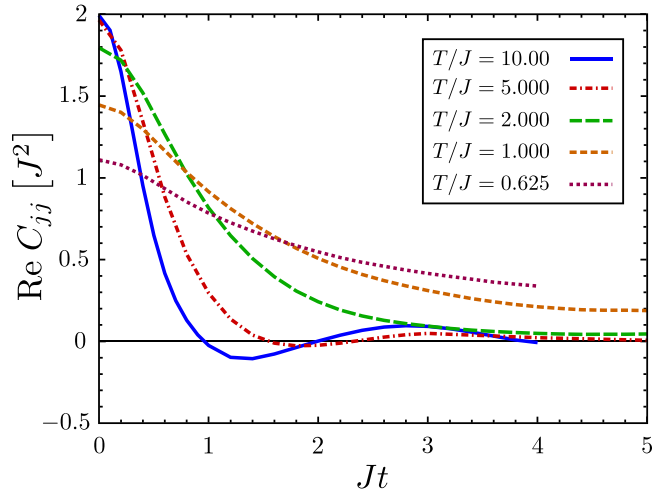

FIG. 4. Time decay of the real part of real-time current-current correlation function at various temperatures for $\omega_0/J = 1$ and $G/J = 0.5$.

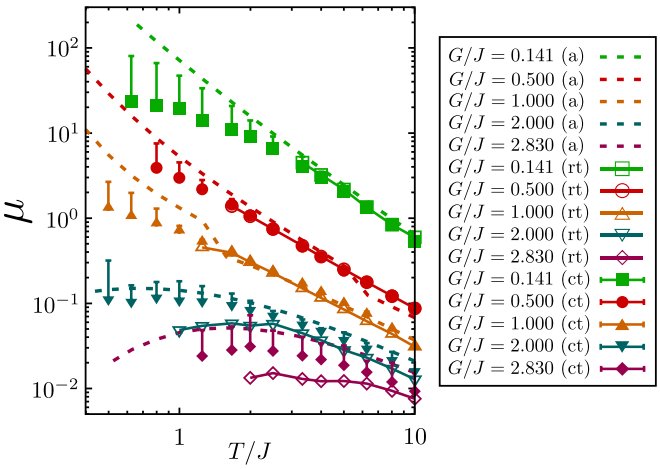

FIG. 5. Temperature dependence of Holstein polaron mobility for different electron-phonon interaction strengths and $\omega_0/J = 1$. The label "ct" stands for the results obtained by analytic continuation from real- and imaginary-time data. Results labeled "rt" are obtained by direct integration of current-current correlation function in real time (full lines connecting the dots are guide to the eye). The results labeled "a" are approximate results from Ref. [72].

adequately smaller N. In particular, we used $N = 20$ for times from $Jt = 5$ to 10 and $N = 30$ for times from $Jt = 10$ to 15.

In Fig. 4 we present the decay of the real part of current-current correlation function in real time for $\omega_0/J = 1$, $G/J = 0.5$ and a range of temperatures. We see that for higher temperatures ($T/J \geqslant 2$) we fully capture the time decay of the current-current correlation function. In that case, it is possible to calculate the mobility by direct integration using the Kubo formula given in Eq. (3). This approach gives us the most accurate results for polaron mobility where the only uncertainty comes from statistical errors of Monte Carlo calculations, which are rather small. The time decay of current-current correlation function for lower temperatures ($T/J < 2$ in this case) is slower and we cannot obtain reliable results at larger times when the dynamical sign problem becomes severe and Monte Carlo statistical errors become significant. In this case, we resort to analytic continuation procedure described in Sec. II C to obtain the result for polaron mobility. That procedure gives results with systematic error that can appear to be significant, especially in the case of low temperatures. In this case, longer real times become more relevant and analytic continuation that makes use only of imaginary-time and short real-time data becomes less successful.

C. Temperature dependence of polaron mobility

We present the final results of our work in this section. The temperature dependence of mobility for one-dimensional Holstein model is presented in Fig. 5. The results are given for electron-phonon interactions ranging from weak ($G/J = 0.141$) to strong ($G/J = 2.830$) and $\omega_0/J = 1$.

The results labeled "ct" in Fig. 5 were obtained from analytic continuation procedure that makes use of imaginary-time data and real-time data up to times where it is possible to obtain Monte Carlo results with small error. The error bars were estimated as follows: We first calculate the relative error that the analytic continuation procedure introduces to real and imaginary-time data generated from dynamic mobility calculated using an approximate method in Ref. [72], as described in Sec. III A. We then assume that the relative error of analytic continuation procedure applied to Monte Carlo data for the same parameter set is the same. This is a good estimate since the current-current correlation functions obtained in Ref. [72] and in this work largely resemble each other. Hence, it is expected that analytic continuation performs equally well for both of these current-current correlation functions. From the relative error, we eventually calculate the estimate of the absolute error of the analytic continuation procedure applied to Monte Carlo data. We find that analytic continuation typically tends to underestimate the mobility. For this reason, we present one-sided errors in Fig. 5.

The results obtained by direct integration in real time for times where reliable current-current correlation function is available are labeled "rt." For reference, we present also the results obtained using an approximate method of Ref. [72] (these are labeled "a").

The most accurate results in this work are the results obtained for relatively weak electron-phonon interactions $G/J \lesssim 1$ and higher temperatures $T/J \gtrsim 2$. For these parameters, we can capture the full time decay of the current-current correlation function and the results obtained by direct integration are therefore accurate. For these parameters, analytic continuation also gives essentially the same results as direct integration.

The path integral for $G/J < 1$ was calculated using the momentum representation for electronic states (see Sec. II B 1). The alternating phase that remains in the integrand is proportional to the factor $\Delta t G$ [see Eq. (16)]. For this reason, the approach works well for weaker interactions, while for large interactions the dynamical sign problem becomes quite severe. We also note that it is a significant challenge to obtain reliable results at low temperatures, because longer times become relevant then, as already discussed in Sec. III B. The other approach based on position representation (described in Sec. II B 2) of electronic states was used to calculate the current-current correlation function in imaginary time, and in real time for interactions $G/J \geqslant 1$.

To illustrate the importance of the choice of basis, we present in Fig. 6(a) the ratio of the standard deviation of the current-current correlation function $C_{jj}(t)$ and its absolute value $|C_{jj}(t)|$ obtained from the calculations using either the position or momentum basis for electronic states. The results are presented up to times when the standard deviation becomes comparable to the result (except for $G/J = 0.5$ and the position basis, where longer times can be reached). As can be seen from the figure, in the case of weak interaction ($G/J = 0.5$), the standard deviation is much smaller when the momentum basis is used, while for strong interaction ($G/J = 2$), the standard deviation is significantly smaller when the position basis is used. To demonstrate that such a behavior originates from variations of phases of the terms in Monte Carlo summation (known as the sign problem in the literature), we present in Fig. 6(b) the average sign of the Monte Carlo sum used to evaluate the nominator in Eq. (12) for the same parameters as in Fig. 6(a). For the sum $\sum_i A_i$ the average sign is defined as $s_{\text{av}} = |\langle A_i/|A_i|\rangle|$. It takes the value of one when there is no sign problem and it is equal to zero

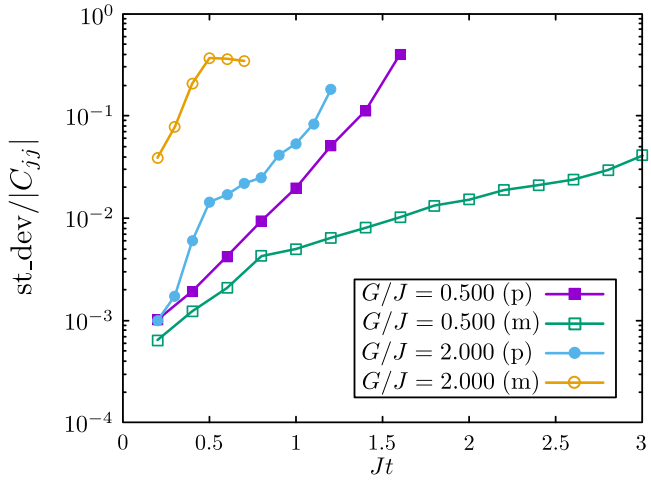

(a)

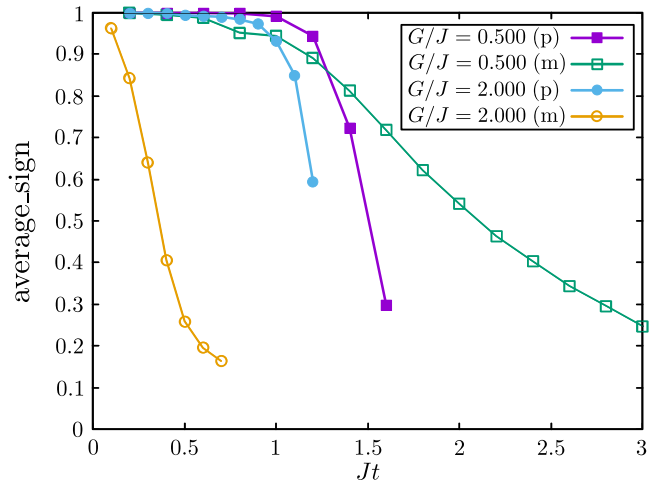

(b)

FIG. 6. The real-time dependence of (a) the relative standard deviation and (b) the average sign of the real-time current-current correlation function for $\omega_0/J = 1$ and $T/J = 2$. The label "m" denotes the results obtained with the momentum representation for electrons and the label "p" denotes the results obtained with the position representation for electrons.

when the sign problem is most severe. We see from Figs. 6(b) and 6(a) that the average sign is close to one in cases where standard deviation is small and that it decreases towards zero at times when standard deviation starts to be comparable to the result.

In Fig. 7 we present the current-current correlation function in imaginary time for $T/J = 1$, $\omega_0/J = 1$, and various values of interaction. We see that it is much more sensitive with respect to (imaginary) time variable for stronger electron-phonon interactions, while for weak electron-phonon interactions it appears to have almost a constant value. Therefore, for weak interactions and low temperatures the results obtained from analytic continuation have large error since the input data on current-current correlation function have very little information (they are almost constant in imaginary time and exhibit a slow decay up to the largest real

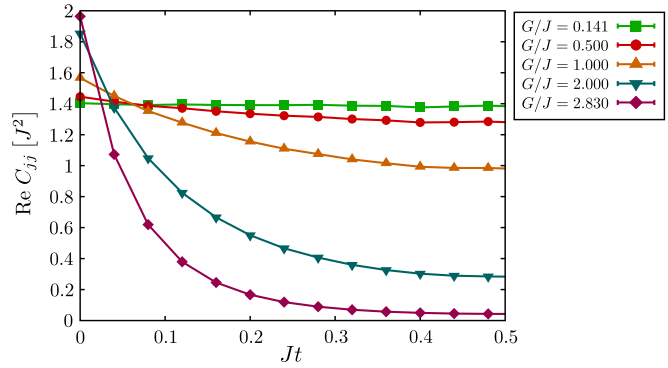

FIG. 7. Imaginary time current-current correlation function for $T/J = 1$, $\omega_0/J = 1$ and for various interaction strengths. The results are shown for imaginary times $0 \leqslant t \leqslant \beta/2$ only since the identity $C_{jj}(t) = C_{jj}(\beta - t)$ holds.

times for which data are available). For weak interactions and high temperatures, the real-time data already contains almost full information on the current-current correlation function. Consequently, analytic continuation gives rather accurate results for these parameters. Analytic continuation also works reasonably well for stronger interactions ($G/J \geqslant 1$). In that case, the current-current correlation function data have a pronounced dependence in imaginary time and for short real times, which gives good enough information to obtain reasonable results from analytic continuation. We note that, for stronger interactions, the mobility obtained by direct integration noticeably underestimates the mobility from analytic continuation. The reason for this is the presence of additional peaks in $C_{jj}(t)$ at times $t_n = n\frac{2\pi}{\omega_0}$ ($n \geqslant 1$) which are not captured by direct integration, as can be seen in Fig. 8.

To summarize for which parameters the methodology presented works best, one can inspect Fig. 5. It can be seen that the error is rather small for relatively weak interactions $G/J \lesssim 1$ and relatively high temperatures $T/J \gtrsim 2$.

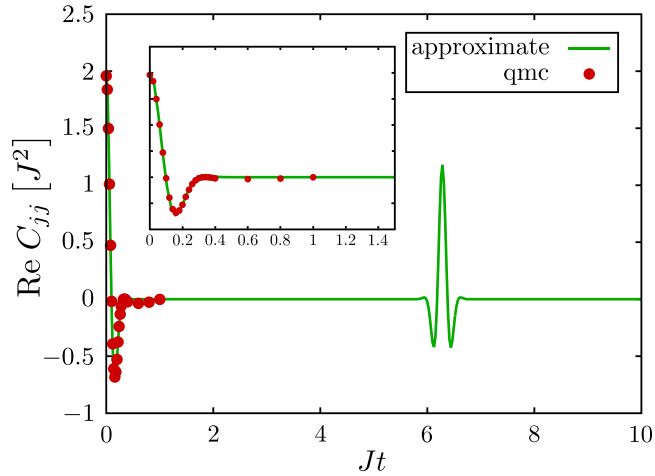

FIG. 8. Time dependence of real part of real-time current-current correlation function for $G/J = 2.83$ and $T/J = 2$ obtained by approximate method from Ref. [72] (labeled "approximate") and by our QMC calculations (labeled "qmc"). The inset shows a detailed view for times $Jt \leqslant 1.5$.

Reasonably accurate results can be also obtained for stronger interactions $G/J > 1$ and relatively high temperatures $T/J \gtrsim 2$. On the other hand, it is quite challenging to obtain the results at low temperatures $T/J < 1$.

It is interesting to compare the results obtained in this work with the results of Ref. [72] obtained using an approximate method. For almost all values of the parameters studied, the results of Ref. [72] fall within the error bar range of the results obtained in this work. Such an agreement establishes the approach of Ref. [72] as a method to obtain reasonably good temperature dependence of the mobility.

We also compare our results to the results of Ref. [68] which is the only reference where the results for temperature dependence of Holstein polaron mobility were reported based on the calculation using the methodology that should be in principle numerically exact. The results of Ref. [68] agree with our results for weakest interaction $G/J = 0.141$ and the temperatures when our estimated error is relatively small. However, for stronger interactions $G/J = 1$, $G/J = 2$, and $G/J = 2.83$ the results of Ref. [68] give lower values of mobility than our results. For example, at $G/J = 2.83$, $\omega_0/J = 1$ and $T/J = 2$ the range of mobility reported in Ref. [68] is $\mu \in (2.8 \times 10^{-3}, 8.1 \times 10^{-3})$, while in our case it is $\mu \in (3.1 \times 10^{-2}, 7.2 \times 10^{-2})$. For these parameters, direct integration around the first peak in current-current correlation function (in the range $0 \leqslant Jt \leqslant 1$ in Fig. 8) gives already $\mu \approx 1.5 \times 10^{-2}$ and the integration around subsequent peaks could only increase this value. The results of Ref. [68] were obtained using analytic continuation of imaginary-time data only and we believe that this analytic continuation might not be sufficiently reliable for all parameter values. This could potentially explain the difference between the results of Ref. [68] and our results.

All the calculations and examples presented in this paper are for a phonon frequency of $\omega_0/J = 1$. We next discuss the effect of phonon frequency on the accuracy and applicability of the methodology. As discussed previously, the methodology performs best when it is possible to perform calculations for real times which are sufficiently long that the current-current correlation function decays toward zero and it is difficult to perform simulations for low temperatures since the correlation function decays rather slowly then. The current-current correlation function is expected to decay more rapidly to zero when the average number of phonons is larger, which happens for smaller phonon energies. Hence, it is expected that it will be possible to reach even lower temperatures in the simulations for smaller phonon energies. On the other hand, for larger phonon energies, the lowest temperature for which simulations can be performed is expected to be larger.

IV. CONCLUSION

In conclusion, we developed the path-integral quantum Monte Carlo methodology for a numerically exact calculation of real- and imaginary-time current-current correlation functions and for the extraction of polaron mobility from these data in systems consisting of an electron interacting with phonons. The appropriate choice of basis for representation of the path-integral-enabled calculations for longer real times. The use of both real- and imaginary-time data enabled more reliable analytic continuation in comparison with the traditional approach where only the imaginary-time data are used. The methodology was applied to the Holstein polaron model and enabled us to obtain reliable results for the temperature dependence of polaron mobility for interactions ranging from weak to strong and for temperatures that are not too low. The overall ideas of the methodology are not restricted to the Holstein polaron model and can be in principle applied to any Hamiltonian describing an electron interacting with phonons.

ACKNOWLEDGMENTS

We thank Veljko Janković, Darko Tanasković, and Petar Mitrić for insightful and stimulating discussions. We acknowledge funding provided by the Institute of Physics Belgrade, through the grant by the Ministry of Science, Technological Development and Innovation of the Republic of Serbia. Numerical computations were performed on the PARADOX-IV supercomputing facility at the Scientific Computing Laboratory, National Center of Excellence for the Study of Complex Systems, Institute of Physics Belgrade.

[1] C. Jacoboni, *Theory of Electron Transport in Semiconductors* (Springer, Berlin, 2010).

[2] N. W. Ashcroft and N. D. Mermin, *Solid State Physics* (Harcourt, Orlando, 1976).

[3] C. Franchini, M. Reticcioli, M. Setvin, and U. Diebold, Polarons in materials, Nat. Rev. Mater. **6**, 560 (2021).

[4] L. R. V. Buizza and L. M. Herz, Polarons and charge localization in metal-halide semiconductors for photovoltaic and light-emitting devices, Adv. Mater. **33**, 2007057 (2021).

[5] B. Guster, P. Melo, B. A. A. Martin, V. Brousseau-Couture, J. C. de Abreu, A. Miglio, M. Giantomassi, M. Côté, J. M. Frost, M. J. Verstraete, and X. Gonze, Fröhlich polaron effective mass and localization length in cubic materials: Degenerate and anisotropic electronic bands, Phys. Rev. B **104**, 235123 (2021).

[6] S. Poncé, W. Li, S. Reichardt, and F. Giustino, First-principles calculations of charge carrier mobility and conductivity in bulk semiconductors and two-dimensional materials, Rep. Prog. Phys. **83**, 036501 (2020).

[7] M. Fiorentini and N. Bonini, Thermoelectric coefficients of *n*-doped silicon from first principles via the solution of the Boltzmann transport equation, Phys. Rev. B **94**, 085204 (2016).

[8] J. Ma, A. S. Nissimagoudar, and W. Li, First-principles study of electron and hole mobilities of Si and GaAs, Phys. Rev. B **97**, 045201 (2018).

[9] S. Poncé, E. R. Margine, and F. Giustino, Towards predictive many-body calculations of phonon-limited carrier mobilities in semiconductors, Phys. Rev. B **97**, 121201(R) (2018).

[10] T.-H. Liu, J. Zhou, B. Liao, D. J. Singh, and G. Chen, First-principles mode-by-mode analysis for electron-phonon scattering channels and mean free path spectra in GaAs, Phys. Rev. B **95**, 075206 (2017).
[11] J.-J. Zhou and M. Bernardi, *Ab initio* electron mobility and polar phonon scattering in GaAs, Phys. Rev. B **94**, 201201(R) (2016).
[12] N. Vukmirović, Calculations of electron mobility in II–VI semiconductors, Phys. Rev. B **104**, 085203 (2021).
[13] T. Holstein, Studies of polaron motion, Ann. Phys. (NY) **8**, 343 (1959).
[14] E. Jeckelmann and S. R. White, Density-matrix renormalization-group study of the polaron problem in the Holstein model, Phys. Rev. B **57**, 6376 (1998).
[15] P. E. Kornilovitch, Continuous-Time Quantum Monte Carlo Algorithm for the Lattice Polaron, Phys. Rev. Lett. **81**, 5382 (1998).
[16] A. H. Romero, D. W. Brown, and K. Lindenberg, Converging toward a practical solution of the Holstein molecular crystal model, J. Chem. Phys. **109**, 6540 (1998).
[17] J. Bonča, S. A. Trugman, and I. Batistić, Holstein polaron, Phys. Rev. B **60**, 1633 (1999).
[18] G. Wellein and H. Fehske, Polaron band formation in the Holstein model, Phys. Rev. B **56**, 4513 (1997).
[19] M. Capone, W. Stephan, and M. Grilli, Small-polaron formation and optical absorption in Su-Schrieffer-Heeger and Holstein models, Phys. Rev. B **56**, 4484 (1997).
[20] G. Wellein and H. Fehske, Self-trapping problem of electrons or excitons in one dimension, Phys. Rev. B **58**, 6208 (1998).
[21] L.-C. Ku, S. A. Trugman, and J. Bonča, Dimensionality effects on the Holstein polaron, Phys. Rev. B **65**, 174306 (2002).
[22] M. Hohenadler, H. G. Evertz, and W. von der Linden, Quantum Monte Carlo and variational approaches to the Holstein model, Phys. Rev. B **69**, 024301 (2004).
[23] S. Ciuchi, F. de Pasquale, S. Fratini, and D. Feinberg, Dynamical mean-field theory of the small polaron, Phys. Rev. B **56**, 4494 (1997).
[24] H. De Raedt and A. Lagendijk, Numerical calculation of path integrals: The small-polaron model, Phys. Rev. B **27**, 6097 (1983).
[25] P. E. Spencer, J. H. Samson, P. E. Kornilovitch, and A. S. Alexandrov, Effect of electron-phonon interaction range on lattice polaron dynamics: A continuous-time quantum Monte Carlo study, Phys. Rev. B **71**, 184310 (2005).
[26] J. Bonča, S. A. Trugman, and M. Berciu, Spectral function of the Holstein polaron at finite temperature, Phys. Rev. B **100**, 094307 (2019).
[27] J. Bonča and S. A. Trugman, Dynamic properties of a polaron coupled to dispersive optical phonons, Phys. Rev. B **103**, 054304 (2021).
[28] D. Jansen, J. Bonča, and F. Heidrich-Meisner, Finite-temperature density-matrix renormalization group method for electron-phonon systems: Thermodynamics and Holstein-polaron spectral functions, Phys. Rev. B **102**, 165155 (2020).
[29] V. Janković and N. Vukmirović, Spectral and thermodynamic properties of the Holstein polaron: Hierarchical equations of motion approach, Phys. Rev. B **105**, 054311 (2022).
[30] P. Mitrić, V. Janković, N. Vukmirović, and D. Tanasković, Spectral Functions of the Holstein Polaron: Exact and Approximate Solutions, Phys. Rev. Lett. **129**, 096401 (2022).
[31] R. P. Feynman, R. W. Hellwarth, C. K. Iddings, and P. M. Platzman, Mobility of slow electrons in a polar crystal, Phys. Rev. **127**, 1004 (1962).
[32] R. P. Feynman, Slow electrons in a polar crystal, Phys. Rev. **97**, 660 (1955).
[33] H. De Raedt and A. Lagendijk, Numerical study of Holstein's molecular-crystal model: Adiabatic limit and influence of phonon dispersion, Phys. Rev. B **30**, 1671 (1984).
[34] D. Thirumalai and B. Berne, Methods for simulating time correlation functions in quantum systems, Comput. Phys. Commun. **63**, 415 (1991).
[35] C. H. Mak and D. Chandler, Solving the sign problem in quantum Monte Carlo dynamics, Phys. Rev. A **41**, 5709 (1990).
[36] G. Cohen, E. Gull, D. R. Reichman, and A. J. Millis, Taming the Dynamical Sign Problem in Real-Time Evolution of Quantum Many-Body Problems, Phys. Rev. Lett. **115**, 266802 (2015).
[37] R. Egger, L. Mühlbacher, and C. H. Mak, Path-integral Monte Carlo simulations without the sign problem: Multilevel blocking approach for effective actions, Phys. Rev. E **61**, 5961 (2000).
[38] D. Kim, J. D. Doll, and D. L. Freeman, Dynamic path integral methods: A maximum entropy approach based on the combined use of real and imaginary-time quantum Monte Carlo data, J. Chem. Phys. **108**, 3871 (1998).
[39] C. H. Mak and R. Egger, A multilevel blocking approach to the sign problem in real-time quantum Monte Carlo simulations, J. Chem. Phys. **110**, 12 (1999).
[40] W. Li, J. Ren, and Z. Shuai, Finite-temperature TD-DMRG for the carrier mobility of organic semiconductors, J. Phys. Chem. Lett. **11**, 4930 (2020).
[41] Y. Tanimura, Numerically "exact" approach to open quantum dynamics: The hierarchical equations of motion (HEOM), J. Chem. Phys. **153**, 020901 (2020).
[42] F. Ortmann, F. Bechstedt, and K. Hannewald, Theory of charge transport in organic crystals: Beyond Holstein's small-polaron model, Phys. Rev. B **79**, 235206 (2009).
[43] F. Ortmann, F. Bechstedt, and K. Hannewald, Charge transport in organic crystals: Interplay of band transport, hopping and electron-phonon scattering, New J. Phys. **12**, 023011 (2010).
[44] Y.-C. Cheng and R. J. Silbey, A unified theory for charge-carrier transport in organic crystals, J. Chem. Phys. **128**, 114713 (2008).
[45] A. Troisi and G. Orlandi, Charge-Transport Regime of Crystalline Organic Semiconductors: Diffusion Limited by Thermal Off-Diagonal Electronic Disorder, Phys. Rev. Lett. **96**, 086601 (2006).
[46] H. Ishii, K. Honma, N. Kobayashi, and K. Hirose, Wave-packet approach to transport properties of carrier coupled with intermolecular and intramolecular vibrations of organic semiconductors, Phys. Rev. B **85**, 245206 (2012).
[47] L. Wang and D. Beljonne, Flexible surface hopping approach to model the crossover from hopping to band-like transport in organic crystals, J. Phys. Chem. Lett. **4**, 1888 (2013).
[48] L. Wang, O. V. Prezhdo, and D. Beljonne, Mixed quantum-classical dynamics for charge transport in organics, Phys. Chem. Chem. Phys. **17**, 12395 (2015).
[49] L. A. Ribeiro and S. Stafström, Impact of the electron-phonon coupling symmetry on the polaron stability and mobility in organic molecular semiconductors, Phys. Chem. Chem. Phys. **18**, 1386 (2016).

[50] L. Song and Q. Shi, A new approach to calculate charge carrier transport mobility in organic molecular crystals from imaginary time path integral simulations, J. Chem. Phys. **142**, 174103 (2015).

[51] M. Kornjača and N. Vukmirović, Polaron mobility obtained by a variational approach for lattice fröhlich models, Ann. Phys. (NY) **391**, 183 (2018).

[52] K. Hannewald, V. M. Stojanović, J. M. T. Schellekens, P. A. Bobbert, G. Kresse, and J. Hafner, Theory of polaron bandwidth narrowing in organic molecular crystals, Phys. Rev. B **69**, 075211 (2004).

[53] P. Mitrić, V. Janković, N. Vukmirović, and D. Tanasković, Cumulant expansion in the Holstein model: Spectral functions and mobility, Phys. Rev. B **107**, 125165 (2023).

[54] N. Prodanović, N. Vukmirović, Z. Ikonić, P. Harrison, and D. Indjin, Importance of polaronic effects for charge transport in CdSe quantum dot solids, J. Phys. Chem. Lett. **5**, 1335 (2014).

[55] S. Fratini and S. Ciuchi, Dynamical Mean-Field Theory of Transport of Small Polarons, Phys. Rev. Lett. **91**, 256403 (2003).

[56] D. Chen, J. Ye, H. Zhang, and Y. Zhao, On the Munn-Silbey approach to polaron transport with off-diagonal coupling and temperature-dependent canonical transformations, J. Phys. Chem. B **115**, 5312 (2011).

[57] Y. Zhao, D. W. Brown, and K. Lindenberg, On the Munn-Silbey approach to nonlocal exciton-phonon coupling, J. Chem. Phys. **100**, 2335 (1994).

[58] R. Levy, J. LeBlanc, and E. Gull, Implementation of the maximum entropy method for analytic continuation, Comput. Phys. Commun. **215**, 149 (2017).

[59] O. Gunnarsson, M. W. Haverkort, and G. Sangiovanni, Analytical continuation of imaginary axis data for optical conductivity, Phys. Rev. B **82**, 165125 (2010).

[60] J. Schött, I. L. M. Locht, E. Lundin, O. Grånäs, O. Eriksson, and I. Di Marco, Analytic continuation by averaging Padé approximants, Phys. Rev. B **93**, 075104 (2016).

[61] H. J. Vidberg and J. W. Serene, Solving the Eliashberg equations by means of n-point Padé approximants, J. Low Temp. Phys. **29**, 179 (1977).

[62] G. Baym and N. D. Mermin, Determination of thermodynamic Green's functions, J. Math. Phys. **2**, 232 (1961).

[63] E. Gallicchio, S. A. Egorov, and B. J. Berne, On the application of numerical analytic continuation methods to the study of quantum mechanical vibrational relaxation processes, J. Chem. Phys. **109**, 7745 (1998).

[64] C. E. Creffield, E. G. Klepfish, E. R. Pike, and S. Sarkar, Spectral Weight Function for the Half-Filled Hubbard Model: A Singular Value Decomposition Approach, Phys. Rev. Lett. **75**, 517 (1995).

[65] M. Jarrell and J. Gubernatis, Bayesian inference and the analytic continuation of imaginary-time quantum Monte Carlo data, Phys. Rep. **269**, 133 (1996).

[66] J. E. Gubernatis, M. Jarrell, R. N. Silver, and D. S. Sivia, Quantum Monte Carlo simulations and maximum entropy: Dynamics from imaginary-time data, Phys. Rev. B **44**, 6011 (1991).

[67] R. N. Silver, D. S. Sivia, and J. E. Gubernatis, Maximum-entropy method for analytic continuation of quantum Monte Carlo data, Phys. Rev. B **41**, 2380 (1990).

[68] A. S. Mishchenko, N. Nagaosa, G. De Filippis, A. de Candia, and V. Cataudella, Mobility of Holstein Polaron at Finite Temperature: An Unbiased Approach, Phys. Rev. Lett. **114**, 146401 (2015).

[69] D. Hangleiter, I. Roth, D. Nagaj, and J. Eisert, Easing the Monte Carlo sign problem, Sci. Adv. **6**, eabb8341 (2020).

[70] G. Mahan, *Many-Particle Physics* (Kluwer Academic, New York, 2000).

[71] See Supplemental Material at http://link.aps.org/supplemental/10.1103/PhysRevB.107.184315 for additional details.

[72] N. Prodanović and N. Vukmirović, Charge carrier mobility in systems with local electron-phonon interaction, Phys. Rev. B **99**, 104304 (2019).